

pubs.acs.org/Macromolecules Article

Role of Distance from Equilibrium in the Fragmentation Kinetics of Block Copolymer Micelles

3 Supriya Gupta, Lucy Liberman, and Timothy P. Lodge*



Cite This: https://doi.org/10.1021/acs.macromol.3c00580



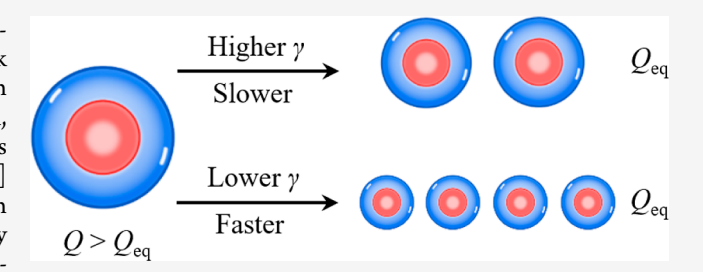
ACCESS I

III Metrics & More

Article Recommendations

SI Supporting Information

4 **ABSTRACT:** The fragmentation kinetics of 1,2-polybutadiene-b-5 poly(ethylene oxide) ($M_{\rm n}=17.2$ kDa and $f_{\rm PEO}=0.38$) block 6 copolymer micelles have been examined with an emphasis on 7 elucidating the role of driving force for micellar fragmentation, 8 represented by the aggregation number ratio $Q/Q_{\rm eq}$. Large micelles 9 with size $Q>Q_{\rm eq}$ were formed in an ionic liquid [$C_{\rm 2}$ mim][TFSI] 10 by the direct dissolution method. A broad range of $Q/Q_{\rm eq}$ was then 11 obtained by altering the solvent quality after micelle formation by 12 addition of a second solvent, selected from a series of imidazolium-13 based ionic liquids [$C_{\rm 2}$ mim][TFSI] with x=2, 4, 6, 8, 10, and 12.



14 In order to quantify the change in solvent quality by dilution, the interfacial tension γ between the different ionic liquids and 1,2-15 polybutadiene homopolymer was determined using the pendant drop method. Micelles in a solution diluted with a second ionic liquid with $x \geq 2$ were equilibrated by high-temperature annealing at 170 °C, during which in situ dynamic light-scattering measurements were made to follow the decay of average micelle size with time. Micelles were further characterized using small-angle 18 X-ray scattering and cryogenic transmission electron microscopy to obtain micelle core size distributions. $Q_{\rm eq}$ and γ were found to 19 exhibit a power-law correlation, $Q_{\rm eq} \sim \gamma^{6/5}$, in accordance with the scaling prediction for star-like micelles. The reduction in γ on 20 dilution with a lower γ solvent (x > 2) results in a smaller equilibrium micelle size, enabling access to a higher $Q/Q_{\rm eq}$, in the range 1 from 1.1 to 5. The rate of fragmentation was found to increase significantly with an increase in $Q/Q_{\rm eq}$, thus the greater 22 thermodynamic driving force leads to a systematic acceleration of fragmentation kinetics. The detailed mechanism by which micelles 23 with $Q \gg Q_{\rm eq}$ achieve $Q_{\rm eq}$ remains to be elucidated; the data suggest that it is not a sequential process but concerted.

24 INTRODUCTION

25 Block copolymers (BCPs) self-assemble into a variety of 26 nanostructures in bulk as well as in solutions with selective 27 solvents. 1-6 Precise control of the polymer block fraction, 28 chain architecture, temperature, concentration, and solvent 29 selectivity results in a myriad of interesting nanostructures, 7-9 30 particularly spherical, cylindrical, or planar micellar par-31 ticles. 10-13 Of particular interest for the present study is 32 core-shell spherical BCP micelles, which find a diverse range 33 of applications in biology, biomedicine, and various industrial 34 processes such as viscosity modification and nanotemplat-35 ing. 14-19 While the equilibrium morphology of micellar 36 structures is well-documented, understanding of the dynamics 37 and mechanisms responsible for the formation and equilibra-38 tion of the micellar structures is still incomplete. 20 A 39 comprehensive picture of the kinetics of micellar relaxation 40 processes is important to realize the full potential of BCP 41 micelles. Concurrently, ionic liquids (ILs) have received 42 increased attention due to their fascinating physico-chemical 43 properties.²¹ ILs can be attractive solvent media for micelle 44 formation because of their superior thermal and chemical 45 stabilities, extremely low vapor pressure, and tunable cohesive 46 energy density.²²

Typically, as-prepared BCP micelles are out of equilibrium 47 and can exhibit a broad size distribution that depends upon the 48 preparation method. Through processes of relaxation, the as- 49 prepared micelles attain a nearly monodisperse equilibrium 50 size. The relaxation can be followed as a function of time by 51 subjecting as-prepared micelles to jumps in temperature, 52 pressure, flow conditions, or solvent quality. Fragmentation, 53 fusion, and single-chain exchange are the key mechanisms 54 responsible for equilibration of BCP micelles. Significant 55 progress has been made toward developing an understanding 56 of the equilibration process of surfactant micelles, both 57 theoretically and experimentally.²³⁻²⁵ Micellar equilibration 58 can be monitored by temperature-jump, pressure-jump, and 59 stopped flow methods. Experimental techniques such as light 60 absorption, fluorescence, small-angle neutron scattering 61 (SANS), and small-angle X-ray scattering (SAXS) have been 62

Received: March 30, 2023 Revised: June 2, 2023



63 employed extensively to study micellar relaxation. ^{26–29} It 64 should be emphasized that the kinetics of BCP micelle 65 relaxation take place over substantially longer timescales 66 (typically ranging from minutes to days) than surfactant 67 micelles (microseconds to milliseconds). ^{30–32} For BCP 68 micelles, notable progress has been made in studying single-69 chain exchange between two micelles when close to 70 equilibrium. ^{33–42} However, the equilibration dynamics of 71 micelles with sizes far from equilibrium remain largely 172 unexplored. ²⁰

Micelles of various sizes can be prepared from a single BCP 74 using different methods of formation, allowing investigation of 75 the relaxation of micelles with sizes on either side of 76 equilibrium. 43 For example, Meli et al. prepared large micelles 77 of 1,2-polybutadiene-b-poly(ethylene oxide) (BO) in 1-ethyl-78 3-methylimidazolium bis(trifluoromethylsulfonyl)imide 79 ([C_2 mim][TFSI]) using a direct dissolution method.⁴⁴ The 80 authors examined the relaxation of these kinetically trapped 81 micelles during prolonged annealing at elevated temperatures 82 by in situ dynamic light scattering (DLS) measurements. The 83 time decay of the normalized average hydrodynamic radius was 84 found to be well-described by an Avrami-type compressed 85 exponential function with an exponent $n \approx 2$ and a 86 characteristic relaxation time of a few hours. 45 More recently, 87 Early and Lodge studied the effect of solvent quality on the 88 relaxation of kinetically trapped similar BO micelles in different imidazolium-based ILs. 46 The relaxation kinetics were found to 90 be independent of solvent quality and concentration, 91 suggesting that the micellar relaxation is dominated by 92 fragmentation, a first-order process. For the same system, 93 time-resolved SANS experiments revealed the absence of 94 significant chain exchange over this time scale even at 200 °C, 95 confirming fragmentation to be the dominant mechanism. 96 Recently, time-resolved liquid-phase transmission electron 97 microscopy (TEM) imaging provided direct evidence of 98 fragmentation. 47 The micelle morphology transitions sequen-99 tially from a large spherical micelle to a prolate spheroid to a 100 "peanut-shaped" particle, which pinches off leading to the 101 creation of daughter micelles. These findings were comple-102 mented with SAXS measurements of average micellar core size. 103 Analogous time-resolved SANS, SAXS, and TEM techniques 104 have been employed previously to examine the kinetics of 105 other morphological transitions in micelles. $^{48-50}$

Previously, kinetic parameters for fusion and fragmentation 107 processes for PEO-*b*-PPO-*b*-PEO in water have been estimated 108 using a fluorescence decay method. 51,52 In addition to 109 experiments, theoretical studies also provide useful insight 110 into the evolution of micelle structure during fragmentation/ 111 relaxation. The characteristic fragmentation time au is 112 conjectured to depend on several parameters such as the size 113 of core- and corona-forming blocks (N_{core} and N_{corona}), the 114 interfacial tension γ between the core-forming block and 115 solvent, the ratio of initial to final micelle aggregation number 116 (Q/Q_{eq}) , and temperature.³² Prior experimental studies have 117 attempted to resolve the dependence of τ on these parameters, 118 yet several questions remain unresolved. In particular, for large 119 micelles, the role of micelle size ratio, Q/Q_{eq} , indicating the 120 departure of the as-prepared micelle size from equilibrium, 121 needs to be examined closely. The ratio Q/Q_{eq} is a measure of 122 the driving force for micellar fragmentation, which could 123 therefore strongly influence the kinetics. The experimental 124 methodology adopted in most prior studies did not allow 125 systematic variation of Q/Q_{eq} over a broad range; rather, it was nearly fixed, typically ca. 1.5 to 2. 45,46 For BO copolymers far 126 from equilibrium, the fragmentation time was reported to 127 depend strongly on the polymer chain size ($\tau \sim N^{1.8}$), but in 128 this case, $Q/Q_{\rm eq} \approx 2$ for each $N^{.53}$ A recent study introduced 129 an experimental methodology that enables variation of $Q/Q_{\rm eq}$ 130 over a broader range, ca. 1.5–6. The protocol involves 131 changing the solvent quality after micelle preparation. As- 132 prepared micelles in $[C_2 {\rm mim}][{\rm TFSI}]$ were diluted with 133 $[C_{10} {\rm mim}][{\rm TFSI}]$ to different degrees of dilution at room 134 temperature, preserving the initial size. Upon subsequent 135 heating, micelles undergo fragmentation in a mixed solvent 136 with lower γ between the micelle core and solvent, which 137 reduced $Q_{\rm eq}$ and thereby increased $Q/Q_{\rm eq}$.

The present study adopts a similar methodology to study the 139 role of $Q/Q_{\rm eq}$ on fragmentation kinetics. The fact that 140 equilibrium micelle size is greatly influenced by γ between 141 the solvent and the core-forming block is used to achieve a 142 variation in Q/Q_{eq} . In the previous study, γ of the solvent 143 medium was varied by varying the amount of the second 144 solvent being added. Here, however, the solvent quality is 145 altered by addition of a second IL chosen from a homologous 146 series with different-length alkyl group (x) on the imidazolium 147 cation [C_xmim][TFSI]; the polymer concentration remains 148 fixed. Since γ controls $Q/Q_{\rm eq}$, measurements of γ between a 149 1,2-polybutadiene (PB) homopolymer and eight different 150 imidazolium-based ILs were made using a pendant drop 151 method. The micelles were characterized by in situ DLS during 152 relaxation following a T-jump to 170 °C. Micelles were further 153 characterized using SAXS and cryo-TEM to estimate the core 154 size and its distribution.

EXPERIMENTAL SECTION

Materials and Characterization. A diblock copolymer, BO, was 157 synthesized previously by anionic polymerization.⁵³ The diblock 158 copolymer is referred to as BO(9-8) with the numbers in parentheses 159 indicating the number-average molecular weight of each block in kDa. 160 Size-exclusion chromatography (SEC) with multiangle light-scattering 161 detection (Wyatt Instruments DAWN) and proton nuclear magnetic 162 resonance spectroscopy (¹H NMR) was performed to determine the 163 polymer number-average molecular weight (M_n) , dispersity (D), and 164 f_{PEO} . For BO(9–8), $M_{\text{n,PB}} = 9.4 \text{ kDa}$, $M_{\text{n,PEO}} = 7.8 \text{ kDa}$, $f_{\text{PEO}} = 0.38$, 165 and D = 1.14. A 1,2-PB homopolymers were synthesized previously, 166 with $M_n = 4.8$ kDa and D = 1.06.53 The following series of ILs was 167 purchased from IoLiTec: 1-methyl-, 1-ethyl-, 1-butyl-, 1-pentyl-, 1- 168 hexyl-, 1-octyl-, 1-decyl-, and 1-dodecyl-3-methylimidazolium bis- 169 (trifluoromethylsulfonyl)imide 99%, denoted as $[C_x mim][TFSI]$, 170 with x = 1, 2, 4, 5, 6, 8, 10, and 12, respectively. The ILs used in 171 the study are molten salts at room temperature. The IL cations and 172 anions consist of bulky, charged small molecules. The chemical 173 structure of IL [C_xmim][TFSI] is presented in Figure 1. The diblock 174 f1 copolymer and all ILs were characterized by ¹H NMR. The ¹H NMR 175 spectrum for the polymer was collected in deuterated chloroform, and 176 spectra for the ILs were obtained in deuterated dimethyl sulfoxide 177 using a Bruker AVANCE HD 500 spectrometer. The Supporting 178 Information contains the SEC chromatograms and NMR spectra for 179 polymers and ILs.

Dynamic Light Scattering. DLS measurements were carried out 181 on micellar samples at room temperature using a multiangle DLS 182 instrument with a Brookhaven BI-200SM goniometer coupled with a 183 Brookhaven BI-9000AT correlator and 637 nm laser source. The in 184 situ DLS experiments at 170 °C were carried out on home-built 185 equipment consisting of a Brookhaven BI-DS photomultiplier 186 mounted onto an adjustable goniometer, equipped with a 488 nm 187 Lexel Ar $^+$ laser and a Brookhaven BI-9000 correlator. Sample 188 temperature was kept within ± 0.5 °C using a silicon oil bath. The 189 samples, made dust-free using 0.45 μm polytetrafluoroethylene filters, 190

156

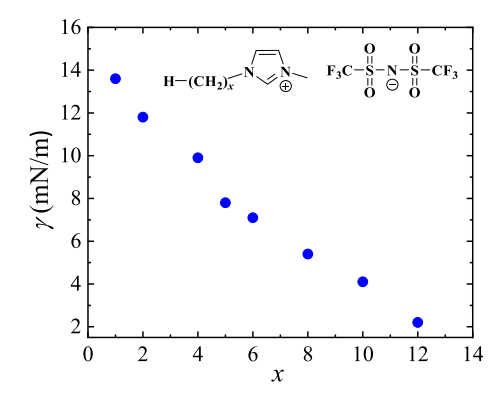


Figure 1. Interfacial tension between 1,2-polybutadiene (PB, M_n = 4.8 kDa) and a series of imidazolium-based ILs [C_x mim][TFSI] at 70 °C. Chemical structure of 1-alkyl-3-methylimidazolium bis-(trifluoromethylsulfonyl imide)-based ILs ([C_x mim][TFSI], where x = 1, 2, 4, 5, 6, 8, 10, and 12).

191 were directly placed into clean oven-dried glass tubes with an ID of 192 5.1 mm. The sample glass tubes were subsequently flame-sealed under 193 vacuum to avoid moisture contact and prevent polymer degradation. 194 Light scattering was performed at multiple angles ranging from 60 to 195 120°, unless otherwise noted. The calculation of the apparent average 196 hydrodynamic radius, $\langle R_h \rangle$, of the micelles from DLS intensity 197 measurement is described in the Supporting Information. The size 198 dispersity, D, is obtained from the reduced second cumulant.

Small-Angle X-ray Scattering. SAXS measurements were 200 performed on micellar solutions before and after fragmentation at 201 room temperature. SAXS measurements were carried out at the 202 Advanced Photon Source, Argonne National Laboratory, on the 203 Sector 5-ID-D beamline. The samples were filled into borosilicate 204 capillaries (diameter 1.5 mm), which were subsequently sealed with 205 epoxy under an argon atmosphere inside a glovebox. 2D SAXS 206 intensity data were collected using a Rayonix MX170-HS CCD area 207 detector with a sample-to-detector distance of 8.5 m. The sample 208 exposure time to X-rays ($\lambda = 0.729 \text{ Å}$) was kept at 0.5 s. By integrating 209 the isotropic 2D scattering data, 1D scattering curves I vs wavevector 210 q were constructed. The background scattering emanating from the 211 solvent and glass capillary was subtracted. The background-212 corrected intensity profiles were fit with a core-shell micelle 213 model; the Percus-Yevick structure factor was used to fit data for 214 the as-prepared micelles. 56,5

Cryogenic Transmission Electron Microscopy. Cryo-TEM imaging was conducted on micelles in both pre- and postfragmentation states. TEM grids with lacey formvar coatings stabilized by carbon were procured from Ted Pella, Inc. Approximately, 0.25 μ L of the sample was drop-casted directly on the TEM grid. The excess solution was removed using filter paper. The sample grid was then manually dropped in liquid nitrogen at around -190 °C prior to imaging. The imaging was performed on FEI Tecnai G2 F30 field-223 emission gun TEM, operated at 300 kV accelerating voltage. A Gatan 224 626 cryo-holder was maintained at -175 °C while imaging. A Gatan 225 UltraScan 4000 4k × 4k CCD camera was used to record digital images. Image analysis was performed using ImageJ software.

Interfacial Tension Measurement. The interfacial tension γ 228 between a series of ILs and the core-forming polymer block PB was 229 determined using pendant drop tensiometry on a Kruss DSA-30S 230 drop shape analyzer as previously described 34 using standard 231 procedures. 58,59 A droplet of IL was suspended in a reservoir of PB 232 homopolymer at 70 °C. Measurements were taken for multiple 233 droplets for a given IL, and for each droplet, multiple frames or 234 measurements were collected. Figure S1 demonstrates the resulting γ 235 values between the PB homopolymer and eight different ILs, i.e., 236 [C_x mim][TFSI] with x = 1, 2, 4, 5, 6, 8, 10, and 12. Step numbers 237 denote the individual measurements taken from multiple droplets. 238 The γ values are listed in Table S1, and the corresponding pendant 239 drop profiles are presented in Figure S2. Each droplet shape

characterizes a particular value of γ . Figure 1 demonstrates the 240 dependence of γ on the length of the alkyl chain on the imidazolium 241 ring, x. As x increases from 1 to 12, γ between PB and the IL 242 decreases monotonically from 13.6 to 2.2 mN/m. Thus, an IL with a 243 higher x becomes comparatively more favorable toward the PB 244 polymer block and the solvent becomes less selective. The key 245 implication of lowering γ is a reduction in equilibrium micelle size 246 O_{OC} :

Sample Preparation. A master micellar solution was prepared by 248 direct dissolution of BO(9–8) in [C₂mim][TFSI], "IL1", with a 249 polymer concentration of 1 wt %. The sample was stirred vigorously 250 at 70 °C for 24–48 h. The solution of as-prepared micelles in 251 [C₂mim][TFSI] was then diluted by the addition of a second IL, 252 "IL2", from the [C_xmim][TFSI] series ($x \ge 2$), reducing the polymer 253 concentration to 0.1 wt %. The dilution was carried out in a careful 254 manner so that the existing micelles remain unchanged in both mean 255 size and distribution. Due to the lower γ for IL2, dilution results in an 256 overall reduction in γ of the solvent mixture surrounding the micelles, 257 amounting to a γ-jump for the as-prepared micelles. After the γ-jump, 258 micelles were heated to 170 °C, followed by annealing, the process 259 being commonly referred to as T-jump, during which micelles attain 260 an equilibrium state, primarily (or even exclusively) through 261 fragmentation.

■ RESULTS AND DISCUSSION

Fragmentation Kinetics in a Single IL. First, fragmenta- 264 tion kinetics were studied for the as-prepared micelles in IL1 265 ([C₂mim][TFSI]). A master solution of 1 wt % BO(9–8) in 266 [C₂mim][TFSI] was prepared. The initial hydrodynamic 267 radius was found to be relatively large ($\langle R_{\rm h} \rangle_{\rm i} \approx 70$ nm) and 268 disperse ($D_{\rm i} \approx 1.27$). The sample was subjected to a T-jump, 269 followed by annealing at 170 °C to approach the equilibrium 270 state, during which the time-dependent average micelle size 271 $\langle R_{\rm h}(t) \rangle$ was measured using in situ DLS. The normalized 272 average hydrodynamic radius of the micelles varying with time, 273 R(t), is expressed using the compressed exponential function 274

$$R(t) = \frac{\langle R_{\rm h}(t) \rangle - \langle R_{\rm h}(\infty) \rangle}{\langle R_{\rm h}(0) \rangle - \langle R_{\rm h}(\infty) \rangle} = \exp[-(t/\tau)^n]$$
(1) ₂₇₅

Here, $\langle R_{\rm h}(0) \rangle = \langle R_{\rm h} \rangle_{\rm i}$ and $\langle R_{\rm h}(\infty) \rangle = \langle R_{\rm h} \rangle_{\rm f}$ represent 276 average hydrodynamic radii of the micelles before and after 277 fragmentation, respectively, τ denotes the characteristic 278 fragmentation time, and n is the exponent. The time 279 dependence of R(t) is presented in Figure S3a. The 280 experimental data were fit to eq 1 to obtain the kinetic 281 parameters τ and n. As-prepared micelles in $[C_2 \text{mim}][\text{TFSI}]$ 282 are found to relax with $\tau = 260$ min and $n \approx 1.7$, in agreement 283 with previous studies. 45,46 The initial micelles equilibrate to 284 generate smaller and relatively narrowly dispersed micelles 285 with $\langle R_{\rm h} \rangle_{\rm f} \approx 29$ nm and $D_{\rm f} \approx 1.02$, as presented in Figure S3b. 286

Fragmentation Kinetics in Mixed ILs. The master 287 solution of 1 wt % as-prepared micelles of BO(9–8) in 288 $[C_2 mim][TFSI]$ was diluted by adding IL2 such that the 289 polymer concentration dropped to 0.1 wt %. Dilution is 290 achieved in a controlled manner such that the size distribution 291 of the as-prepared micelles remains unchanged. Altering the 292 solvent quality by the addition of a lower γ solvent, referred to 293 as γ-jump, was followed by a T-jump to induce fragmentation. 294 As with IL1 alone, micelles approach equilibrium during high-295 temperature annealing, and R(t) was monitored by in situ 296 DLS. Figure 2 displays the average micelle size as a function of 297 to 298 [C₂mim][TFSI] to [C₁₂mim][TFSI], the decay curves 299 progressively shift to the left, indicating faster kinetics. For 300

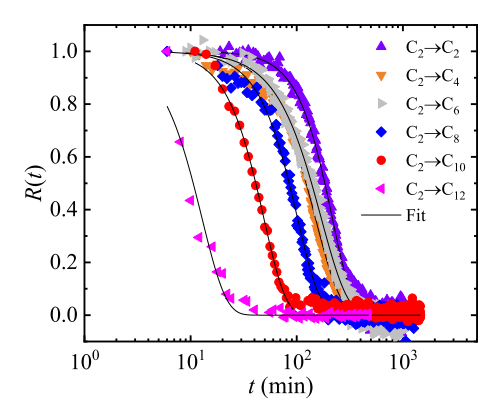


Figure 2. Time decay of the normalized average hydrodynamic radius R(t) of the BC micelles in different pairs of mixed ILs at 170 °C. The solid lines represent best fits to eq 1. The polymer concentration was fixed at 0.1 wt %.

301 all IL2s, the experimental data fit the Avrami expression (eq 1) 302 well. The resulting two kinetic parameters, τ and n, are 303 summarized in Table 1. The initial size of the micelles is 304 essentially independent of dilution (except for [C₁₂mim]-305 [TFSI], which possibly initiates some fragmentation at room 306 temperature). The as-prepared micelles with size around 70 307 nm attain near-equilibrium sizes that depend on the choice of $_{308}$ IL2: $\langle R_{\rm h} \rangle_{\rm f}$ gradually decreases from 29 to 22 nm as the IL2 is 309 changed from $[C_2mim][TFSI]$ to $[C_{12}mim][TFSI]$. After 310 relaxation, the micelle size distribution becomes quite narrow, 311 with $D_f \leq 1.03$ for all IL2s. The corresponding regularized 312 positive exponential sum (REPES) analysis is presented in 313 Figure S4. Interestingly, the characteristic fragmentation time, 314 τ , is found to decrease significantly upon dilution with a 315 progressively lower γ solvent: as x increases from 2 to 12, τ 316 decreases from 216 to 10 min. Whereas τ decreases, the 317 exponent $n \approx 2$ irrespective of IL2.

To further characterize the micelles before and after 319 relaxation, SAXS measurements were carried out to obtain 320 the average micelle core radius $\langle R_{\rm core} \rangle$, which provides an 321 estimate of the mean micelle aggregation number Q. Figure 3a 322 shows I(q) profiles for 1% BO(9-8) micelles in pure $[C_2 \text{mim}]$ TFSI, before and after fragmentation. The spherical 324 form factor is clearly evident in both cases. The micelle core 325 radius can be calculated from the first minimum in I(q) as 326 $\langle R_{\rm core} \rangle \approx 4.493/q_{\rm min}$. A shift to a larger value for $q_{\rm min}$ indicates 327 a decrease in $\langle R_{\rm core} \rangle$ after fragmentation. Based on $\langle R_{\rm core} \rangle$ 328 values obtained from SAXS for the as-prepared micelles $(\langle R_{\text{core}} \rangle) = 17.4 \text{ nm}$, the average aggregation number for 330 micelles before fragmentation was determined to be $Q \approx 1350$, 331 assuming the micellar core to be solvent-free. After 332 fragmentation, the average aggregation number attains an 333 equilibrium value of $Q_{\rm eq} \approx 1275$. Thus, the initial size ratio Q/ $Q_{\rm eq}$ for the equilibration of as-prepared micelles in [$C_{\rm 2}$ mim]- 334 [TFSI] is estimated to be around 1.1. This modest change 335 suggests that many of the initial micelles do not, in fact, 336 undergo any fragmentation in this solvent.

SAXS measurements were also carried out for the micelles 338 equilibrated after dilution. It should be noted that for the 339 diluted samples, the characteristics of the micelles before 340 fragmentation are assumed to be the same as those for the as- 341 prepared micelles in IL1, depicted in Figure 3a. Figure 3b 342 shows the background-corrected I(q) curves for the micelles 343 after fragmentation for different IL2s. As IL2 changes from 344 $[C_2mim][TFSI]$ to $[C_{12}mim][TFSI]$, the first minimum in 345 I(q) shifts to larger q, indicative of decreasing $\langle R_{core} \rangle$. $\langle R_{core} \rangle_{f}$ 346 and $\sigma_{\rm core}$ (standard deviation of the core radius) were obtained 347 by fitting I(q) profiles with the core-shell model.⁵⁶ The 348 decrease in $\langle R_{core} \rangle_f$ upon dilution with an IL with larger x 349 reflects the decrease in γ of the solvent mixture. Table 2 350 t2 summarizes the micelle characteristics estimated from SAXS. 351 $\langle R_{\rm core} \rangle_{\rm f}$ decreases from 17 nm for IL2 having x=2 to 10 nm $_{352}$ when IL2 with x = 12; σ_{core} remains small for all IL1–IL2 pairs. 353 Consequently, Q_{eq} decreases from 1250 to 260 as micelles 354 undergo fragmentation in solvents with progressively lower γ 355 values. Since Q is fixed for all the diluted samples, the ratio of 356 aggregation numbers, Q/Q_{eo} increases from 1.1 to 5.2 as IL2 is 357 changed from [C₂mim][TFSI] to [C₁₂mim][TFSI]. Thus, 358 diluting the micellar solution with a progressively less-polar IL2 359 renders the as-prepared micelles further from the equilibrium 360 size, indicating an enhancement in driving force for 361 fragmentation. It should be noted that in the calculation of 362 Q_{eq} , the assumption of solvent-free core may not hold for a 363 lower γ solvent such as $[C_{12}mim][TFSI]$. However, the 364 difference is expected to be within the uncertainty for the ratio 365

Cryo-TEM imaging was also conducted to confirm the 367 spherical nature of the micelles as well as to obtain the core 368 size and its distribution. Imaging was performed on the 369 micellar solutions before and after fragmentation. Representa- 370 tive micrographs for 1% BO(9–8) in $[C_2 mim][TFSI]$ before 371 and after thermal annealing at 170 °C are presented in Figure 372 f4 4a,c, respectively. The bright regions are micelle cores, 373 f4 embedded in a dark matrix representing corona and solvent. 374 Evidently, micelles are spherical and relatively uniform in size. 375 The structural details such as micellar core size and 376 distribution were obtained by analyzing the micrographs. 377 Image analysis provides a histogram for the distribution in 378 micelle core size; about 400 micelles were taken into 379 consideration in each case. Figure 4b,d depicts the histograms 380 before and after fragmentation, respectively. The continuous 381 curves represent a lognormal distribution constructed using the 382 mean and standard deviation values for each case. The average 383 micellar core radius $\langle R_{\rm core} \rangle$ for the as-prepared micelles is 384

Table 1. Micelle Fragmentation Parameters from DLS

$(P + IL1) \rightarrow I$	L2 $\langle R_{\rm h} \rangle_{\rm i} \ {\rm nm}$	D_{i}	$\langle R_{\rm h} \rangle_{\rm f}$ nm	$D_{ m f}$	au (min)	n
C_2	71	1.27	29	1.02	260 ± 20	1.7
$C_2 \rightarrow C_2$	70	1.20	27	1.02	216 ± 25	2.2
$C_2 \rightarrow C_4$	67	1.17	28	1.01	150 ± 10	1.8
$C_2 \rightarrow C_6$	67	1.20	26	1.02	170 ± 20	1.7
$C_2 \rightarrow C_8$	62	1.15	24	1.01	100 ± 20	2.0
$C_2 \rightarrow C_{10}$	67	1.17	23	1.02	50 ± 10	2.0
$C_2 \rightarrow C_{12}$	40	1.10	22	1.01	10 ± 5	2.1

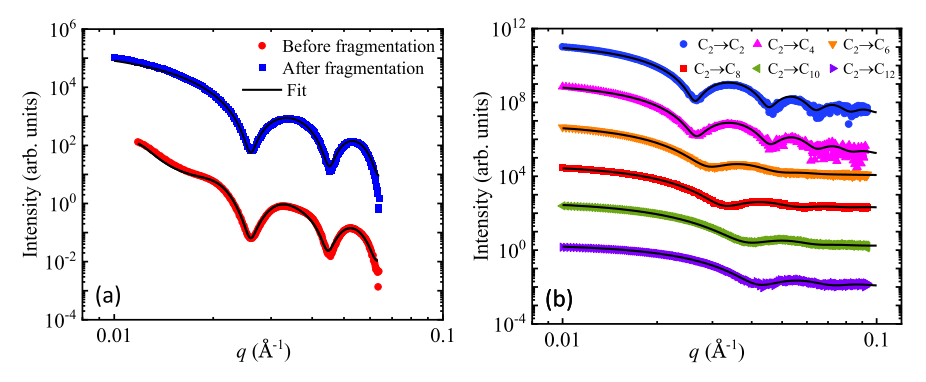


Figure 3. (a) SAXS intensity profiles for 1 wt % BO(9–8) micelles in pure $[C_2 \text{mim}][\text{TFSI}]$ at 25 °C, before and after fragmentation. (b) I(q) versus q for 0.1 wt % BO(9–8) in different pairs of ILs after fragmentation at 25 °C. The curves are shifted vertically by factors of 10^2 for clarity.

Table 2. Micelle Characteristics after Fragmentation from SAXS

$(P + IL1) \rightarrow IL2$	$\langle R_{\rm core} \rangle_{\rm f} (\rm nm)$	$\sigma_{ m core} \ ({ m nm})$	$Q_{\rm eq}$	$Q/Q_{\rm eq}$
C_2	17.1	0.7	1275	1.1
$C_2 \rightarrow C_2$	17	0.7	1250	1.1
$C_2 \rightarrow C_4$	16.8	0.8	1210	1.1
$C_2 \rightarrow C_6$	15.2	1.5	900	1.5
$C_2 \rightarrow C_8$	13.3	0.8	600	2.3
$C_2 \rightarrow C_{10}$	11.6	1	400	3.4
$C_2 \rightarrow C_{12}$	10.1	0.7	260	5.2

385 estimated to be 17 nm. After relaxation, the size distribution 386 becomes slightly narrower ($\sigma_{\rm core} = 0.8$) and $\langle R_{\rm core} \rangle$ decreases to 387 16 nm. The TEM estimates for $\langle R_{\rm core} \rangle$ are therefore in close 388 agreement with those calculated from SAXS.

Cryo-TEM imaging was also performed on the micelles quilibrated in the mixed ILs. Figure 5a-f presents the

micrographs along with the corresponding histograms for 391 different IL2s. The predominantly spherical shapes of the 392 micelles are again evident. As the IL2 changes from $[C_2\text{mim}]$ 393 to $[C_{12}\text{mim}]$, implying reduction in γ of the solution mixture 394 from 11 to 3 mN/m, $\langle R_{\text{core}} \rangle_{\text{f}}$ decreases substantially from 395 around 16 to 9 nm. Note also that as IL2 changes from 396 $[C_2\text{mim}]$ to $[C_{12}\text{mim}]$, the change in electron density in the 397 solvent mixture leads to weaker contrast, especially with $x \geq 8$. 398 Micelle characteristics obtained from cryo-TEM are summarized in Table 3. As noted earlier, micelles undergoing 400 t3 fragmentation in a solvent medium with a lower γ result in 401 progressively smaller micelles at equilibrium. The significant 402 reduction in Q_{eq} leads to an enhancement in the size ratio Q/ 403 Q_{eq} , which increases from around 1.2–6; these estimates from 404 cryo-TEM are consistent with those calculated from SAXS. 405

Figure 6 demonstrates the dependence of $Q_{\rm eq}$ on γ ; $Q_{\rm eq}$ 406 f6 decreases significantly as γ is progressively reduced on dilution 407 with IL with higher x. The driving force for larger micelles is 408

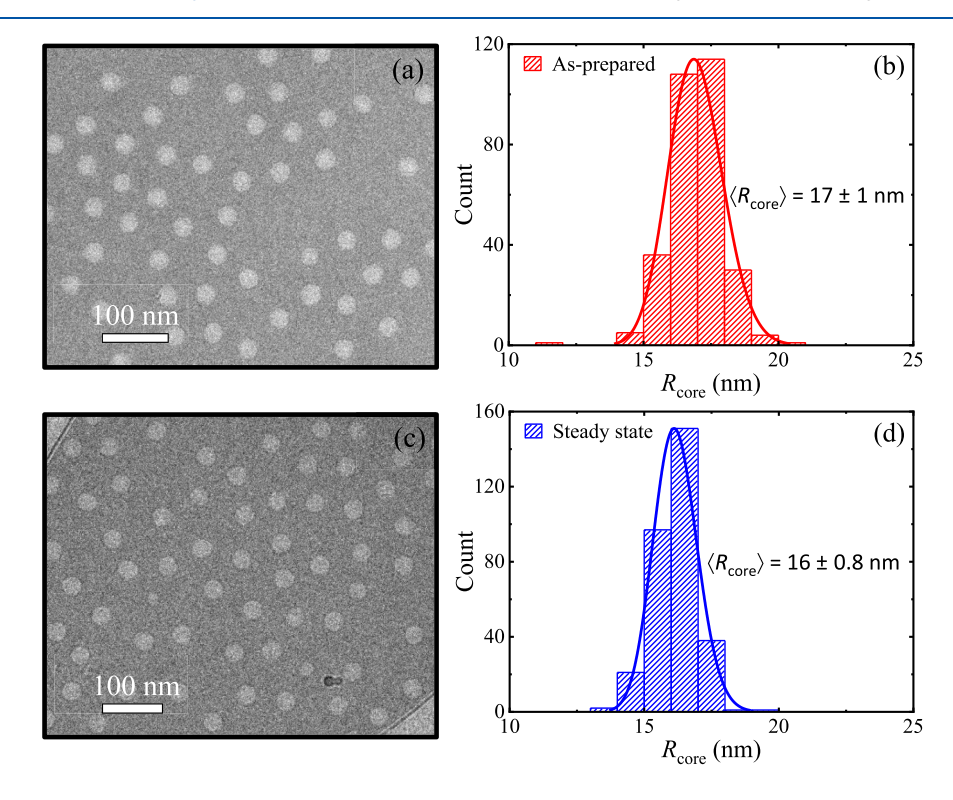


Figure 4. Cryo-TEM electron micrographs and their respective histograms of micellar core radius for 1 wt % BO(9–8) in $[C_2mim][TFSI]$ (master solution). Micelle cores appear as bright regions: (a,b) before fragmentation and (c,d) after fragmentation.

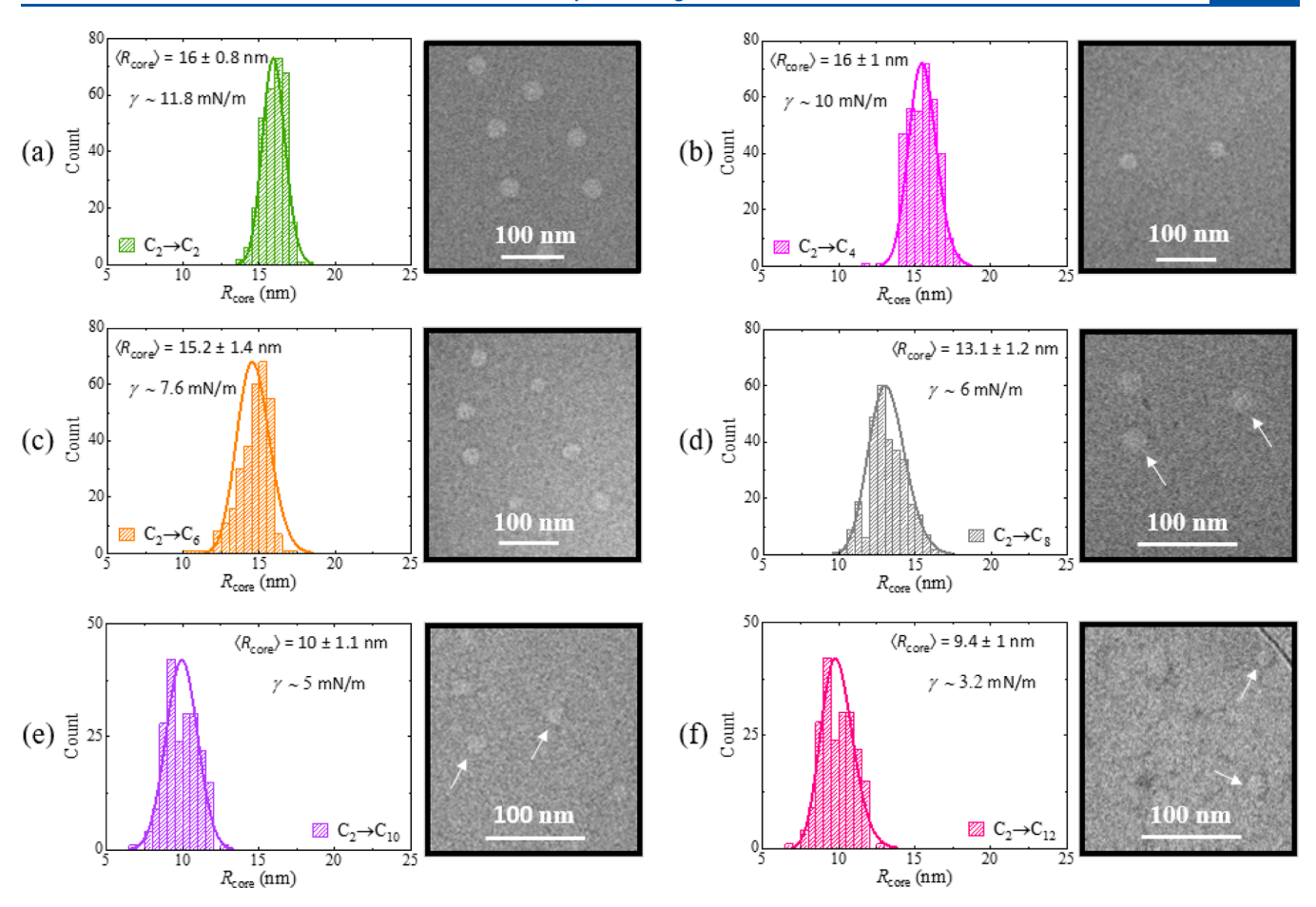


Figure 5. TEM micrographs and the corresponding histograms for the core radius distribution of 0.1 wt % BO(9–8) micelles after relaxation in mixed ILs. (a) $C_2 \rightarrow C_2$; (b) $C_2 \rightarrow C_4$ (c) $C_2 \rightarrow C_6$; (d) $C_2 \rightarrow C_8$; (e) $C_2 \rightarrow C_{10}$; and (f) $C_2 \rightarrow C_{12}$.

Table 3. Micelle Characteristics after Fragmentation from Cryo-TEM

$(P + IL1) \rightarrow IL2$	$\langle R_{\rm core} \rangle_{\rm f} \ ({\rm nm})$	$\sigma_{ m core} \ (m nm)$	$Q_{\rm eq}$	$Q/Q_{\rm eq}$
C ₂	16.1	0.8	1070	1.2
$C_2 \rightarrow C_2$	16	0.8	1040	1.2
$C_2 \rightarrow C_4$	16	1.1	1040	1.2
$C_2 \rightarrow C_6$	15.2	1.4	900	1.4
$C_2 \rightarrow C_8$	13.1	1.2	580	2.2
$C_2 \rightarrow C_{10}$	10	1.1	260	5
$C_2 \rightarrow C_{12}$	9.4	1.0	210	6

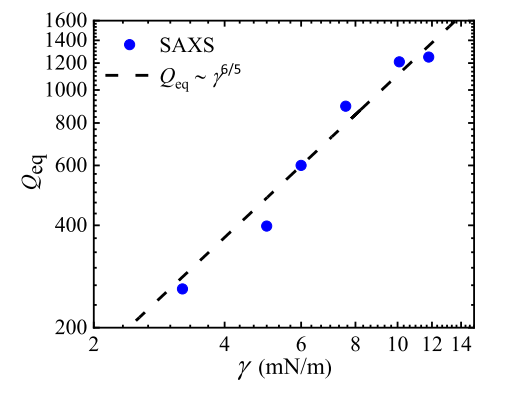


Figure 6. Dependence of equilibrium micelle size, $Q_{\rm eq}$ on solvent quality γ . Symbols represent data obtained from SAXS. The dashed line represents scaling prediction for star-like micelles, $Q_{\rm eq} \sim \gamma^{6/5}$.

the interfacial free energy (proportional to γ); however, the 409 counterbalancing core and corona stretching entropy penalty 410 differs between theoretical approaches. ^{11,60,61} For star-like 411 micelles (Halperin model¹⁰) $Q_{\rm eq} \sim \gamma^{6/5}$, whereas for crew-cut 412 micelles (planar brush model, based on work by de Gennes⁶¹ 413 and Alexander⁶²), $Q_{\rm eq} \sim \gamma^{18/11}$. In comparison, mean-field 414 theory gives $Q_{\rm eq} \sim \gamma^{.5,12}$ In Figure 6, fitting $Q_{\rm eq}$ with γ reveals a 415 power-law dependence, $Q_{\rm eq} \sim \gamma^{1.2 \pm 0.1}$, consistent with the 416 scaling prediction by Halperin for star-like micelles. ¹⁰ The 417 experimental data have been fitted with all three theoretical 418 predictions for comparison, as displayed in Figure S17. 419 Additionally, $Q_{\rm eq}$ vs γ correlation is consistent with our 420 previous results, ⁵⁴ as compared in Figure S18. Note that in the 421 previous study, γ was varied in mixtures of two ILs attained by 422 varying the amount of low γ solvent added (and thus polymer 423 concentration), whereas in the present study, γ is varied by the 424 addition of a second IL chosen from a homologous series with 425 different-length alkyl groups on the imidazolium cation at fixed 426 polymer concentration.

As noted above, for all pairs (except for C_2-C_{12}) of mixed 428 ILs, the as-prepared micelles (in IL1) remain unaffected on 429 dilution with IL2 at room temperature. Thus, the aggregation 430 number before equilibration, denoted by Q_i is held nearly 431 constant for all pairs of ILs studied. The reduction in Q_{eq} , 432 therefore, allows systematic variation of the ratio Q/Q_{eq} , and 433 thus the driving force for fragmentation. Figure 7 shows the 434 f7 variation in fragmentation time with Q/Q_{eq} . The fragmentation 435 time decreases significantly, and monotonically, with increasing 436

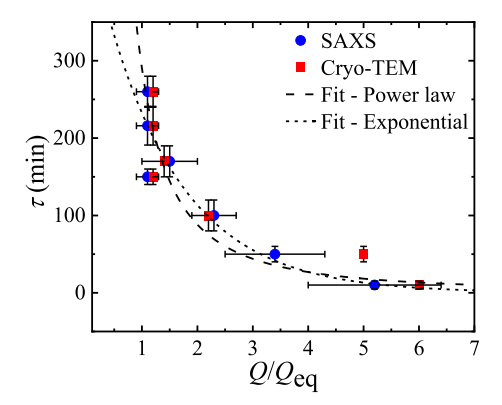


Figure 7. Dependence of characteristic fragmentation time, τ , on micelle size ratio $Q/Q_{\rm eq}$. The error bars denote the standard error in τ and $Q/Q_{\rm eq}$ (propagated from $R_{\rm core}$). Dashed and dotted lines represent power law and exponential fit to SAXS data.

437 driving force. Two empirical curve fits are also shown, one an 438 exponential $[\tau \sim \exp{(-0.3~Q/Q_{\rm eq})}]$ and one a power-law $(\tau \sim$ 439 $(Q/Q_{\rm eq})^{-1.7})$ both providing reasonable descriptions of the 440 data; we are not aware of a theoretical model that might be 441 compared to the results. The enhanced rate of fragmentation 442 can be attributed to a greater thermodynamic drive to attain 443 equilibrium as micelles much larger than the equilibrium size 444 are energetically less stable. Kinetically, therefore, the 445 relaxation process becomes faster for micelles farther from 446 the equilibrium state.

TEM imaging provides the core size distribution of micelles before (as-prepared) and after equilibration (steady state). Higher 8a displays an overlay of the micelle count distributions as a function of Q (obtained from cryo-TEM) before and after fragmentation in pure $[C_2 \text{mim}][\text{TFSI}]$ (no dilution). The assignmentation in pure exhibit a broad distribution in size. Prolonged thermal annealing at 170 °C drives the initial micelles to relax to approach Q_{eq} . In the case of no dilution, micelles are prepared and fragmented in the same IL. Hence, the initial size ratio Q/Q_{eq} , which is calculated as 1.1 from SAXS, remains fixed. Since Q/Q_{eq} is not very high, the shift in micelle size distribution due to fragmentation is relatively small. In fact, as noted previously, a significant fraction of the initial micelle population does not undergo fragmentation. Unfortunately, DLS does not provide direct access to the fraction of micelles that have undergone fragmentation at any

The present study aims to achieve a broader variation in $Q/Q_{\rm eq}$, which is realized by dilution of the as-prepared micelles

with a lower γ solvent before thermal annealing. Figure 8b 466 demonstrates the shift in micelle core size distribution due to 467 fragmentation under altered solvent quality vis-à-vis as- 468 prepared micelles. Figure 8b displays the overlayed micelle 469 size distributions from cryo-TEM at equilibrium (after 470 fragmentation) for different pairs of IL1-IL2. It should be 471 noted that for all solvent pairs, the initial micelle distribution is 472 the same, indicated by the dashed curve. The distribution shifts 473 toward lower Q after fragmentation. While the shift is less 474 prominent for dilution with IL2 having x = 2, it becomes 475 progressively more and more prominent when the solution is 476 diluted by the addition of lower γ ILs (x > 2). As confirmed in 477 Figure 6, the smaller equilibrium micelle size for dilution with 478 IL having higher x is correlated with the reduction in γ . The 479 relatively small shifts in size distribution upon dilution with 480 either $[C_2 \text{mim}][TFSI]$ (x = 2) or $[C_4 \text{mim}][TFSI]$ (x = 4) 481 indicate that only a small fraction of micelles experience 482 fragmentation, presumably the ones with $Q/Q_{eq} > 1$; micelles 483 with size $Q \leq Q_{eq}$ remain intact. However, when micelles are 484 diluted with IL2 having x = 6, 8, 10, or 12, the value of Q_{eq} 485 decreases significantly, and hence, most or all micelles across 486 the initial distribution undergo fragmentation. In fact, for 487 dilution with $[C_{10}mim][TFSI]$ or $[C_{12}mim][TFSI]$, the entire 488 initial distribution shifts to lower Q. This corresponds to a 489 significant enhancement in the average size ratio Q/Q_{eq} , from 490 1.1 to 5.2. A significant shift in Q and its distribution suggests 491 that micelles far above the equilibrium size undergo a series of 492 fragmentation events to achieve equilibrium. For example, if 493 $Q/Q_{eq} \approx$ 4, it is possible that a given micelle fragments once to $_{494}$ give two micelles with $Q/Q_{eq} \approx 2$, and these "daughter" 495 micelles then undergo secondary fragmentation events to yield 496 four micelles with $Q \approx Q_{eq}$. In this scenario, one might expect 497 the net fragmentation time to be greater than, or equal to, that 498 for micelles prepared with $Q/Q_{eq} \approx$ 2, with equality 499 corresponding to the situation where a micelle with $Q/Q_{eq} \approx 500$ 4 fragments much more rapidly than one with $Q/Q_{eq} \approx 2$. The 501 data in Figure 7 do not support this mechanism; however, 502 micelles with $Q/Q_{eq} \ge 4$ achieve equilibrium more rapidly than 503 those with $Q/Q_{eq} \approx 2$, suggesting that the process for $Q/Q_{eq} \geq 504$ 4 bypasses an intermediate state with $Q/Q_{eq} \approx 2$. Possibilities 505 include a large micelle "extruding" multiple daughter micelles 506 with $Q/Q_{eq} \approx 1$ or spontaneously breaking into more than two 507 daughter micelles. To explore these possibilities, in situ time- 508 resolved liquid-phase TEM measurements are an attractive 509 option. While it is confirmed that the chain-exchange process is 510 very slow compared to fragmentation of BO(9-8) micelles in 511 $[C_2 \text{mim}][TFSI]^{45}$ for lower γ solvents, especially $[C_{12} \text{mim}]$ - 512

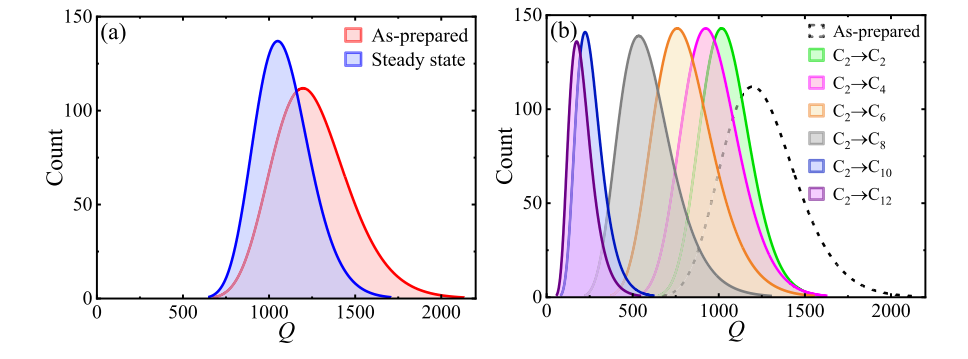


Figure 8. Overlayed count distributions of BO(9–8) micelles as a function of Q from cryo-TEM: (a) in pure $[C_2 mim][TFSI]$ and (b) in different pairs of IL1–IL2 after fragmentation.

Macromolecules Article pubs.acs.org/Macromolecules

513 [TFSI], the role of chain-exchange processes in micellar 514 relaxation needs to be investigated separately. Even though the s15 relaxation of big micelles of size $Q/Q_{eq} \gg 1$ is believed to be 516 driven mainly by micellar fragmentation, the presence of chain 517 exchange in solution diluted with [C₁₂mim][TFSI] cannot be 518 completely ruled out.

519 **SUMMARY**

520 Fragmentation kinetics of spherical micelles of 1,2-polybuta-521 diene-b-poly(ethylene oxide) diblock copolymers have been 522 investigated in strategically mixed solvents made of imidazo-523 lium-based ILs. The jump in solvent quality achieved by the 524 addition of a second solvent after the formation of micelles in a 525 first solvent influences the equilibrium micelle size and hence ₅₂₆ the fragmentation behavior. Relatively large $(\langle R_h \rangle_i \approx 70 \text{ nm})$ s27 and dispersed ($D_i \approx 1.27$) initial micelles were prepared by the 528 direct dissolution of BO(9-8) in a higher γ IL ([C₂mim]-529 [TFSI]), followed by dilution with a second IL with a lower γ 530 ([C_x mim][TFSI] with x > 2). Micelles under the altered 531 solvent medium attain equilibrium after prolonged thermal 532 annealing at 170 °C, resulting in smaller and narrowly 533 dispersed micelles after equilibration. In particular, progressive 534 reduction in γ , achieved by selecting a second IL with an 535 increasing value of x, tends to decrease the equilibrium micelle $_{536}$ size, characterized by $\langle R_h \rangle_{\!f}$ by DLS, $\langle R_{core} \rangle_{\!f},$ by SAXS, and 537 cryo-TEM, and therefore Q_{eq}. In situ DLS experiments 538 demonstrate that the characteristic fragmentation time of 539 BO(9–8) micelles can be lowered substantially by decreasing γ 540 of the surrounding medium after micelle formation. An 541 increase in size ratio Q/Q_{eo} , which represents the extent of 542 driving force for fragmentation, is responsible for faster 543 fragmentation. Micelle fragmentation in a single IL, irre-544 spective of its γ value, exhibits only a narrow Q/Q_{eq} around 545 1.1–1.5 in the absence of γ -jump. However, a notable variation 546 in the micelle size ratio Q/Q_{eq} from 1.1 to 5.2 was achieved 547 using the γ -jump strategy adopted in the present study. A 548 significant decrease in micelle core size indicates fragmentation 549 to be the primary mechanism for equilibration. While for $_{550}$ micelles close to equilibrium (with Q/Q_{eq} just above unity), 551 only a fraction of micelles experience fragmentation, and for ss2 larger micelles (with $Q/Q_{eq} > 2$), the entire population of the 553 as-prepared micelle appears to undergo fragmentation. 554 Fragmentation of such big micelles may take place through a 555 series of multiple fragmentation events or by a more concerted 556 process; there is some evidence for the latter. Finally, the study 557 indicates that the fragmentation time can be tuned by 558 controlled variation in solvent quality after micelle preparation.

ASSOCIATED CONTENT

560 Supporting Information

563

564

565

567

568

569

570

561 The Supporting Information is available free of charge at 562 https://pubs.acs.org/doi/10.1021/acs.macromol.3c00580.

> Pendant drop profiles of ILs, R(t) versus time of 1% BO(9-8) in pure $[C_2mim][TFSI]$, micelle size distributions using REPES, SAXS profile of BO(9-8) in bulk, ¹H NMR spectra of BO(9–8) and all ILs, SEC-RI traces of PB(4.8k) and BO(9-8) in tetrahydrofuran, IL parameters, Q_{eq} vs γ and τ vs Q/Q_{eq} for BO(9–8) in mixed ILs, core-shell model equations, and contrast values (PDF)

AUTHOR INFORMATION

Corresponding Author

Timothy P. Lodge – Department of Chemistry and Department of Chemical Engineering and Materials Science, 574 University of Minnesota, Minneapolis, Minnesota 55455-0431, United States; o orcid.org/0000-0001-5916-8834; Email: lodge@umn.edu

571

572

575

576

577

578

579

580

581

582

584

585

588

589

608

Authors

Supriya Gupta – Department of Chemistry, University of Minnesota, Minneapolis, Minnesota 55455-0431, United States; o orcid.org/0000-0002-0105-3855

Lucy Liberman - Department of Chemistry, University of Minnesota, Minneapolis, Minnesota 55455-0431, United

Complete contact information is available at: https://pubs.acs.org/10.1021/acs.macromol.3c00580

587

The authors declare no competing financial interest.

ACKNOWLEDGMENTS

This work was funded by the National Science Foundation 590 Polymers Program through award DMR-2103630. SAXS 591 experiments were performed at the 5-ID-D beamline of the 592 Dupont-Northwestern-Dow Access Team (DND-CAT) at the 593 Advanced Photon Source (APS), Argonne National Labo- 594 ratory. Use of the APS, an Office of Science User Facility 595 operated for the U.S. Department of Energy (DOE) Office of 596 Science by Argonne National Laboratory, was supported by 597 the U.S. DOE under contract no. DE-AC02-06CH11357. The 598 authors are grateful to Prof. Lorraine Francis for facilitating use 599 of the KRUSS DSA-30S tensiometer and Prof. Lynn Walker 600 for helpful discussion. The authors acknowledge the Character- 601 ization Facility, College of Science and Engineering, University 602 of Minnesota, which receives partial support from the NSF 603 through the MRSEC (award number DMR-2011401) and the 604 NNCI (award number ECCS-2025124) programs. The 605 homopolymer and copolymer used were provided by Dr. 606 Julia Early.

REFERENCES

- (1) Gohy, J. F. Block Copolymer Micelles. Adv. Polym. Sci. 2005, 609 190, 65-136.
- (2) Mai, Y.; Eisenberg, A. Self-Assembly of Block Copolymers. 611 Chem. Soc. Rev. 2012, 41, 5969-5985.
- (3) Tritschler, U.; Pearce, S.; Gwyther, J.; Whittell, G. R.; Manners, 613 I. 50th Anniversary Perspective: Functional Nanoparticles from the 614 Solution Self-Assembly of Block Copolymers. Macromolecules 2017, 615 50, 3439-3463. 616
- (4) Gupta, S.; Chokshi, P. Self-Organization of a 4-Miktoarm Star 617 Block Copolymer Induced by Cylindrical Confinement. Soft Matter 618 **2021**, *17*, 4929-4941.
- (5) Noolandi, J.; Hong, K. M. Theory of Block Copolymer Micelles 620 in Solution. *Macromolecules* **1983**, *16*, 1443–1448.
- (6) Lodge, T. P. Block Copolymers: Long-Term growth with Added 622 Value. Macromolecules 2020, 53, 2-4. 623
- (7) Bates, F. S.; Fredrickson, G. H. Block Copolymers—Designer 624 Soft Materials. Phys. Today 1999, 52, 32-38.
- (8) Matsen, M. W.; Schick, M. Stable and Unstable Phases of a 626 Diblock Copolymer Melt. Phys. Rev. Lett. 1994, 72, 2660-2663. 627
- (9) Fredrickson, G. H. The Equilibrium Theory of Inhomogeneous 628 Polymers; Oxford University Press, 2013.

- 630 (10) Halperin, A. Polymeric Micelles: A Star Model. *Macromolecules* 631 **1987**, 20, 2943–2946.
- 632 (11) Halperin, A.; Tirrell, M.; Lodge, T. P. Tethered Chains in 633 Polymer Microstructures. *Adv. Polym. Sci.* **1992**, *100*, 31–71.
- 634 (12) Nagarajan, R.; Ganesh, K. Block Copolymer Self-Assembly in 635 Selective Solvents: Spherical Micelles with Segregated Cores. *J. Chem.* 636 *Phys.* **1989**, *90*, 5843–5856.
- 637 (13) Zhulina, E. B.; Adam, M.; LaRue, I.; Sheiko, S. S.; Rubinstein, 638 M. Diblock Copolymer Micelles in a Dilute Solution. *Macromolecules* 639 **2005**, 38, 5330–5351.
- 640 (14) Hubbell, J. A. Enhancing Drug Function. *Science* **2003**, *300*, 641 595–596.
- 642 (15) Elsabahy, M.; Heo, G. S.; Lim, S. M.; Sun, G.; Wooley, K. L. 643 Polymeric Nanostructures for Imaging and Therapy. *Chem. Rev.* 2015, 644 115, 10967–11011.
- 645 (16) Ge, Z.; Liu, S. Functional Block Copolymer Assemblies 646 Responsive to Tumor and Intracellular Microenvironments for Site-647 Specific Drug Delivery and Enhanced Imaging Performance. *Chem.* 648 Soc. Rev. **2013**, 42, 7289–7325.
- 649 (17) Gupta, S.; Chokshi, P. Self-Assembly of Polymer Grafted 650 Nanoparticles within Spherically Confined Diblock Copolymers. *J.* 651 *Phys. Chem. B* **2020**, *124*, 11738–11749.
- 652 (18) Krishnamoorthy, S.; Pugin, R.; Brugger, J.; Heinzelmann, H.; 653 Hinderling, C. Nanopatterned Self-Assembled Monolayers by Using 654 Diblock Copolymer Micelles as Nanometer-Scale Adsorption and 655 Etch Masks. *Adv. Mater.* **2008**, *20*, 1962–1965.
- 656 (19) Wang, T. Y.; Tsiang, R. C. C.; Liou, J. S.; Wu, J.; Sheu, H. C. 657 Preparation and Characterization of a Star-Shaped Polystyrene-*b*-658 Poly(Ethylene-*co*-Propylene) Block Copolymer as a Viscosity Index 659 Improver of Lubricant. *J. Appl. Polym. Sci.* **2001**, 79, 1838–1846.
- 660 (20) Lodge, T. P.; Seitzinger, C. L.; Seeger, S. C.; Yang, S.; Gupta, 661 S.; Dorfman, K. D. Dynamics and Equilibration Mechanisms in Block 662 Copolymer Particles. *ACS Polym. Au* **2022**, *2*, 397–416.
- 663 (21) Lodge, T. P. A Unique Platform for Materials Design. *Science* 664 **2008**, 321, 50-51.
- 665 (22) He, Y.; Li, Z.; Simone, P.; Lodge, T. P. Self-Assembly of Block 666 Copolymer Micelles in an Ionic Liquid. *J. Am. Chem. Soc.* **2006**, *128*, 667 2745–2750.
- 668 (23) Zana, R. Dynamics in Micellar Solutions of Amphiphilic Block 669 Copolymers. In *Dynamics of Surfactant Self-Assemblies: Micelles,* 670 Microemulsions, Vesicles, and Lyotropic Phases; Hubbard, A. T., Ed.;
- 671 Taylor & Francis Group/CRC Press: Boca Raton, 2005, pp 161–231. 672 (24) Aniansson, E. A. G.; Wall, S. N. Kinetics of Step-Wise Micelle
- 672 (24) Aniansson, E. A. G.; Wall, S. N. Kinetics of Step-Wise Micelle 673 Association. J. Phys. Chem. 1974, 78, 1024–1030.
- 674 (25) Aniansson, E. A. G.; Wall, S. N.; Almgren, M.; Hoffmann, H.;
- 675 Kielmann, I.; Ulbricht, W.; Zana, R.; Lang, J.; Tondre, C. Theory of 676 the Kinetics of Micellar Equilibria, and Quantitative Interpretation of
- 677 Chemical Relaxation Studies of Micellar Solutions of Ionic
- 678 Surfactants. J. Phys. Chem. 1976, 80, 905–922.
- 679 (26) Wang, Y.; Balaji, R.; Quirk, R. P.; Mattice, W. L. Detection of 680 the Rate of Exchange of Chains between Micelles Formed by Diblock 681 Copolymers in Aqueous Solution. *Polym. Bull.* **1992**, 28, 333–338.
- 682 (27) Cao, T.; Munk, P.; Ramireddy, C.; Tuzar, Z.; Webber, S. E. 683 Fluorescence Studies of Amphiphilic Poly(Methacrylic Acid)-Block-
- 684 Polystyrene-Block-Poly(Methacrylic Acid) Micelles. *Macromolecules* 685 **1991**, 24, 6300–6305.
- 686 (28) Smith, C. K.; Liu, G. Determination of the Rate Constant for 687 Chain Insertion into Poly(Methyl Methacrylate)-Block-Poly-688 (Methacrylic Acid) Micelles by a Fluorescence Method. *Macro-*
- 688 (Methacrylic Acid) Micelles by a Fluorescence Method. *Macro-*689 molecules **1996**, 29, 2060–2067. 690 (29) Willner, L.; Poppe, A.; Allgaier, J.; Monkenbusch, M.; Richter, 691 D. Time-Resolved SANS for the Determination of Unimer Exchange
- D. Time-Resolved SANS for the Determination of Unimer Exchange
 Kinetics in Block Copolymer Micelles. *Europhys. Lett.* 2001, 55, 667–693
 673.
- 694 (30) Halperin, A.; Alexander, S. Polymeric Micelles: Their 695 Relaxation Kinetics. *Macromolecules* 1989, 22, 2403–2412.
- 696 (31) Halperin, A. On Micellar Exchange: The Role of the Insertion 697 Penalty. *Macromolecules* **2011**, 44, 5072–5074.

- (32) Dormidontova, E. E. Micellization Kinetics in Block Copolymer 698 Solutions: Scaling Model. *Macromolecules* **1999**, 32, 7630–7644. 699
- (33) Won, Y. Y.; Davis, H. T.; Bates, F. S. Molecular Exchange in 700 PEO-PB Micelles in Water. *Macromolecules* **2003**, *36*, 953-955.
- (34) van Stam, J.; Creutz, S.; De Schryver, F. C.; Jérôme, R. Tuning 702 of the Exchange Dynamics of Unimers between Block Copolymer 703 Micelles with Temperature, Cosolvents, and Cosurfactants. *Macro-704 molecules* **2000**, *33*, 6388–6395.
- (35) Lu, J.; Bates, F. S.; Lodge, T. P. Remarkable Effect of Molecular 706 Architecture on Chain Exchange in Triblock Copolymer Micelles. 707 *Macromolecules* **2015**, 48, 2667–2676. 708
- (36) Choi, S.; Lodge, T. P.; Bates, F. S. Mechanism of Molecular 709 Exchange in Diblock Copolymer Micelles: Hypersensitivity to Core 710 Chain Length. *Phys. Rev. Lett.* **2010**, *104*, 047802.
- (37) Zhao, D.; Ma, Y.; Lodge, T. P. Exchange Kinetics for a Single 712 Block Copolymer in Micelles of Two Different Sizes. *Macromolecules* 713 **2018**, *51*, 2312–2320.
- (38) Ma, Y.; Lodge, T. P. Chain Exchange Kinetics in Diblock 715 Copolymer Micelles in Ionic Liquids: The Role of χ. Macromolecules 716 **2016**, 49, 9542–9552.
- (39) Seeger, S. C.; Dorfman, K. D.; Lodge, T. P. Free Energy 718 Trajectory for Escape of a Single Chain from a Diblock Copolymer 719 Micelle. ACS Macro Lett. 2021, 10, 1570–1575.
- (40) Wang, E.; Zhu, J.; Zhao, D.; Xie, S.; Bates, F. S.; Lodge, T. P. 721 Effect of Solvent Selectivity on Chain Exchange Kinetics in Block 722 Copolymer Micelles. *Macromolecules* **2019**, *53*, 417–426.
- (41) Lund, R.; Willner, L.; Stellbrink, J.; Radulescu, A.; Richter, D. 724 Role of Interfacial Tension for the Structure of PEP–PEO Polymeric 725 Micelles. A Combined SANS and Pendant Drop Tensiometry 726 Investigation. *Macromolecules* **2004**, *37*, 9984–9993.
- (42) Lund, R.; Willner, L.; Richter, D.; Dormidontova, E. E. 728 Equilibrium Chain Exchange Kinetics of Diblock Copolymer Micelles: 729 Tuning and Logarithmic Relaxation. *Macromolecules* **2006**, 39, 4566–730 4575.
- (43) Cameron, N. S.; Corbierre, M. K.; Eisenberg, A. 1998 E.W.R. 732 Steacie Award Lecture Asymmetric amphiphilic block copolymers in 733 solution: a morphological wonderland. *Can. J. Chem.* **1999**, 77, 1311–734 1326.
- (44) Meli, L.; Lodge, T. P. Equilibrium vs Metastability: High- 736 Temperature Annealing of Spherical Block Copolymer Micelles in an 737 Ionic Liquid. *Macromolecules* **2009**, 42, 580–583.
- (45) Meli, L.; Santiago, J. M.; Lodge, T. P. Path-Dependent 739 Morphology and Relaxation Kinetics of Highly Amphiphilic Diblock 740 Copolymer Micelles in Ionic Liquids. *Macromolecules* **2010**, 43, 741 2018–2027.
- (46) Early, J. T.; Lodge, T. P. Fragmentation of 1,2-Polybutadiene- 743 Block-Poly(Ethylene Oxide) Micelles in Imidazolium-Based Ionic 744 Liquids. *Macromolecules* **2019**, 52, 7089–7101.
- (47) Early, J. T.; Yager, K. G.; Lodge, T. P. Direct Observation of 746 Micelle Fragmentation via In Situ Liquid-Phase Transmission 747 Electron Microscopy. ACS Macro Lett. 2020, 9, 756–761.
- (48) Lund, R.; Willner, L.; Richter, D.; Lindner, P.; Narayanan, T. 749 Kinetic Pathway of the Cylinder-to-Sphere Transition in Block 750 Copolymer Micelles Observed in Situ by Time-Resolved Neutron and 751 Synchrotron Scattering. ACS Macro Lett. 2013, 2, 1082–1087.
- (49) Wang, L.; Huang, H.; He, T. Rayleigh Instability Induced 753 Cylinder-to-Sphere Transition in Block Copolymer Micelles: Direct 754 Visualization of the Kinetic Pathway. ACS Macro Lett. 2014, 3, 433–755 438.
- (50) Parent, L. R.; Bakalis, E.; Ramírez-Hernández, A.; Kammeyer, J. 757 K.; Park, C.; de Pablo, J.; Zerbetto, F.; Patterson, J. P.; Gianneschi, N. 758 C. Directly Observing Micelle Fusion and Growth in Solution by 759 Liquid-Cell Transmission Electron Microscopy. *J. Am. Chem. Soc.* 760 **2017**, 139, 17140–17151.
- (51) Rharbi, Y. Fusion and Fragmentation Dynamics at Equilibrium 762 in Triblock Copolymer Micelles. *Macromolecules* **2012**, 45, 9823–763 9826.
- (52) Landazuri, G.; Fernandez, V. V. A.; Soltero, J. F. A.; Rharbi, Y. 765 Length of the Core Forming Block Effect on Fusion and Fission 766

Macromolecules Article pubs.acs.org/Macromolecules

- 767 Dynamics at Equilibrium in PEO-PPO-PEO Triblock Copolymer
- 768 Micelles in the Spherical Regime. Macromolecules 2021, 54, 2494-769 2505.
- (53) Early, J. T.; Block, A.; Yager, K. G.; Lodge, T. P. Molecular 770
- Weight Dependence of Block Copolymer Micelle Fragmentation
- 772 Kinetics. J. Am. Chem. Soc. 2021, 143, 7748-7758.
- (54) Gupta, S.; Lodge, T. P. Effect of Changing Interfacial Tension
- 774 on Fragmentation Kinetics of Block Copolymer Micelles. Macro-
- 775 molecules 2023, 56, 2137-2148.
- (55) Araque, J. C.; Hettige, J. J.; Margulis, C. J. Modern Room
- 777 Temperature Ionic Liquids, a Simple Guide to Understanding Their
- 778 Structure and How It May Relate to Dynamics. J. Phys. Chem. B 2015, 779 119, 12727-12740.
- 780 (56) Guinier, A.; Fournet, G.; Yudowitch, K. L. Small-Angle 781 Scattering of X-Rays; Wiley: New York, 1955.
- (57) Pedersen, J. S. Determination of size distribution from small-782
- 783 angle scattering data for systems with effective hard-sphere
- 784 interactions. J. Appl. Crystallogr. 1994, 27, 595-608.
- (58) Berry, J. D.; Neeson, M. J.; Dagastine, R. R.; Chan, D. Y.;
- 786 Tabor, R. F. Measurement of Surface and Interfacial Tension using
- 787 Pendant Drop Tensiometry. J. Colloid Interface Sci. 2015, 454, 226-788 237.
- (59) Bashforth, F.; Adams, J. C. An Attempt to Test the Theories of 789
- 790 Capillary Action by Comparing the Theoretical and Measured Forms of
- 791 Drops of Fluid; University Press, 1883.
- (60) Izzo, D.; Marques, C. M. Formation of Micelles of Diblock and 792
- 793 Triblock Copolymers in a Selective Solvent. Macromolecules 1993, 26,
- 795 (61) de Gennes, P.-G. Scaling Theory of Polymer Adsorption. J. 796 Phys. (Paris) 1976, 37, 1445-1452.
- (62) Alexander, S. Adsorption of Chain Molecules with a Polar Head
- 798 a Scaling Description. J. Phys. (Paris) 1977, 38, 983-987.